Buckling and Post-Buckling Behavior of Lipped-Channel Columns Undergoing Distortional-Global Interaction at Elevated Temperatures

Elisson B. Ferreira Filho[1], Alexandre Landesmann[1], Dinar Camotim[2]

[1]*Programa de Engenharia Civil, PEC/COPPE/UFRJ, Universidade Federal do Rio de Janeiro*
Av. Athos da Silveira Ramos-149. Centro de Tecnologia – Bloco B, Sala 101, 21941-909, Rio de Janeiro, Brazil
elisson.filho@coc.ufrj.br, alandes@coc.ufrj.br
[2] *CERIS, DECivil, Instituto Superior Técnico, Universidade de Lisboa*
Av. Rovisco Pais, 1049-001, Lisboa, Portugal
dcamotim@civil.ist.utl.pt

Abstract. This study investigates the behavior of cold-formed steel fixed-ended lipped-channel columns undergoing distortional-global (D-G) interaction at high temperatures. It extends the scope of previous works by including columns exposed to temperatures up to 800º C due to fire conditions with a different temperature-dependent material model. The columns' dimensions and lengths were chosen to provide true D-G interaction. ABAQUS shell finite element analyses were conducted to obtain elastic-plastic post-buckling equilibrium paths, failure loads, and collapse modes for these columns. The AZ/NZS 4600 (2018) constitutive model was employed to account for the steel behavior at high temperatures. Several room-temperature yield stresses were considered to cover a wide slenderness range. The numerical failure loads provided insights for further studies, including remarks to be taken into account in the future proposals of DSM-based curves, more specifically in the sense of considering the effects caused by the variation of the non-linearity of the steel stress-strain curves with temperature.

Keywords: Cold-formed Steel Columns, Distortional-global Interaction, Buckling, Post-Buckling.

1 Introduction

Cold-formed steel (CFS) columns have been increasingly employed in the construction industry due to several advantages such as low weight-to-strength ratio, great versatility in producing complex shapes, and low erection costs. However, the high slenderness of CFS members leads to the development of instability phenomena, namely local (L), distortional (D), and global (G) buckling modes or by coupling (interaction) between them (L-D, D-G, L-D-G). Figure 1(a) shows a lipped-channel section (LC) and its "pure" buckled cross-sectional shapes (Figure 1(b)-(e)) – note that lipped-channel columns may globally buckle by flexural-torsional (FT) or minor-axis flexural (Fm) modes, depending on the column length.

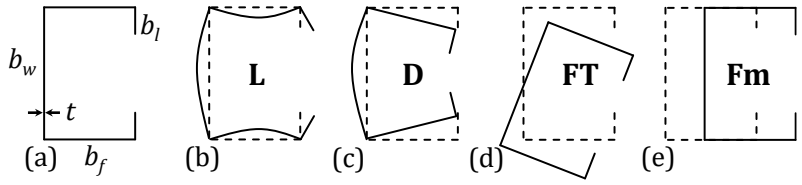

Figure 1. Lipped channel: (a) section dimensions and buckled cross-section shapes corresponding to (b) local, (c) distortional, (d) flexural-torsional, and (e) minor axis flexural buckling modes.

According to Dinis *et al.* [1], D-G interaction may occur if the column distortional and global critical buckling loads (P_{crD} and P_{crG}, respectively) are close enough, provided that P_y is sufficiently high to allow the corresponding buckling modes to compete/erode the column strength – $P_y = A \cdot f_y$ is the squash load where A is the cross-section area and f_y is the yield strength at room temperature (20°C). Numerical studies involving LC columns [1]–[4] showed that when the global-to-distortional critical buckling loads ratio ($R_{GD} = P_{crG}/P_{crD}$) is comprised between 0.90 and 1.0, more pronounced is the erosion of column strength, the so-called "true D-G interaction" range. However, even with R_{GD} values out of this range, if $P_y >> \max\{P_{crD};P_{crG}\}$ the interaction may still occur through secondary distortional or global bifurcations – SDI for if $R_{GD}<0.9$, or SGI if $R_{GD}>1.10$, respectively.

The distortional and global (flexural-torsional – FT) post-buckling behaviors in CFS columns (including LC sections) at elevated temperatures were previously studied separately by Landesmann *et al.* [5] and Bicelli *et al.* [6], respectively. These authors assessed the available design approaches (based on the Direct Strength Method – DSM, e.g., [7]) and proposed new sets of DSM curves to handle columns failing in D and FT modes. In recent investigations, conducted by Ferreira Filho *et al.* [8], [9], a similar approach was used to study the post-buckling behavior, strength and DSM design of fixed-ended LC columns prone to D-G (precisely D-FT) interaction at elevated temperatures. These three works evaluated columns failing at elevated temperatures up to 800°C and used the EC3:1-2 [10] material model to simulate the steel temperature-dependent material behavior. The combined failure data gathered by these authors showed that the column strengths were greatly influenced by the material response at elevated temperatures, i.e., by the constitutive model adopted.

In fact, several studies concerning CFS columns at elevated temperatures, whether numerical and/or experimental, have shown that the post-buckling behavior and strength of the columns are greatly affected by the steel temperature-dependent stress-strain relationship (e.g.,[11]–[16]). In terms of standard codes, in addition to EC3:1-2 [10], another one that provides a constitutive model for CFS at high temperatures is AS/NZS 4600 [17] (Australian/New Zealand), described in Section 3.1. Figure 2(a) makes it possible to qualitatively compare the constitutive models prescribed in these codes, showing the variation of Young's modulus, yield stress and proportionality limit stress reduction factors with temperature ($k_E = E_T/E_{20}$, $k_y = f_{yT}/f_y$ and $k_p = f_{pT}/f_y$, respectively) – note that AS/NZS provides different k_y values for low-strength steels (LSS) and high-strength (HSS), while k_p values are given only in EC3. As for Figure 2(b), it shows f_T/f_y *vs.* ε plots for T = 20/100-400-600 °C, where a given stress at temperature T (f_T) is normalized with respect to its room-temperature yield stress counterpart (f_y). Based on Figure 2 it can be noted that: (i) the k_y factors related to LSS and HSS are very different from each other, as well as from those prescribed in EC3; (ii) this assertion can be extended for the k_E values, which are also very different from code to code, (iii) there is a noticeable ("intriguing") similarity between the curves for LSS k_y factors and the EC3 k_p ones, and, finally, (iv) it can be noted that there is a relatively greater proximity between LSS and EC3 stress-strain curves (mostly for $T \leq 400$ °C), in comparison with the HSS ones, which develop very distinct paths.

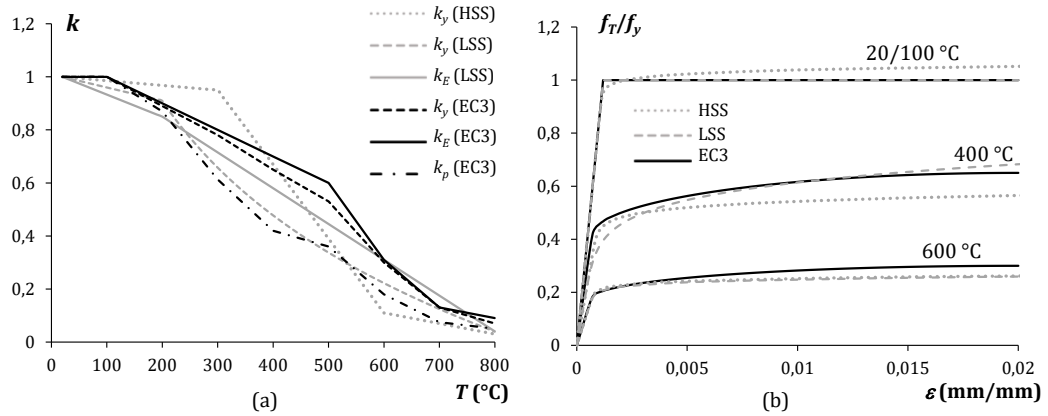

Figure 2. Comparison between AS/NZS 4600 [17] and EC3:1-2 [10] CFS constitutive models: (a) reduction factors, and (b) normalized stress-strain curves for T = 20-400-600°C.

In this context, the present work, still in its initial phase, is inserted to provide data to investigate the effect caused by another temperature-dependent material model in the buckling and elastic-plastic post-buckling behavior of steel columns of LC cross-sections under elevated temperatures. For this purpose, a similar approach as adopted in [5], [6], [8], [9] is used, however, the material model considered will be the one given in the AS/NZS [17] standard, allowing obtaining the structural response of steel under high temperatures. The results collected here will serve as a basis for future studies that aim to provide a DSM-based strength curve for columns in D-G interaction both under room and at elevated temperatures.

2 Buckling behavior – column geometry selection

The LC fixed-ended columns studied in this work were previously selected in [8] through a series of "trial-and-error" elastic buckling analyses performed in GBTul [18] – based on Generalized Beam Theory (GBT) – in

order to ensure high susceptivity to D-FT interactions (true interactions), both at room and elevated temperatures. Table 1 displays the 12 LC geometries (b_w, b_f, b_l and t in mm– see Figure 1(a)), lengths L (mm), the β_{FT} geometrical parameter and relevant critical loads (kN) and ratios.

Table 1. Selected LC column geometries, critical buckling loads and relevant buckling load ratios (mm and kN).

Column	b_w	b_f	b_l	t	A	β_{FT}	L	P_{crFT}	P_{crD}	R_{GD}	P_{crL}	$P_{crL}/P_{cr.Max}$
LC1	150	130	10	4.20	1806	4.35	5000	325	407	0.80	1459	3.58
LC2	130	115	10	3.55	1349	4.30	4000	278	309	0.90	994	3.22
LC3	100	80	15	5.00	1450	3.59	1450	1381	1430	0.97	3865	2.70
LC4	90	90	10	3.00	870	3.39	2250	270	276	0.98	810	2.93
LC5	140	140	13	3.50	1561	4.00	4500	290	293	0.99	869	2.97
LC6	100	100	10	3.50	1120	3.29	2500	348	351	0.99	1173	3.34
LC7	150	130	13	4.00	1744	4.46	4150	434	436	1.00	1293	2.97
LC8	100	90	15	5.00	1550	3.13	1550	1269	1273	1.00	3591	2.82
LC9	90	80	10	3.00	810	3.85	2000	316	316	1.00	871	2.75
LC10	120	100	10	4.50	1530	3.91	2500	671	650	1.03	2114	3.15
LC11	120	140	12	3.02	1280.5	3.43	4000	216	195	1.11	553	2.56
LC12	100	120	10	2.96	1065.6	3.00	2900	230	192	1.20	603	2.62

Figure 3(a) displays signature curves for LC8 at four temperatures 20-400-600-800 °C providing the variation elastic critical buckling load at temperature T (P_{crT}) with length (L − logarithmic scale). The AS/NZS CFS constitutive model, addressed in Section 3.1, is adopted and all buckling loads are calculated for E_{20} = 210 GPa (steel Young's modulus at room temperature) and ν = 0.3 (Poisson's ratio, deemed temperature independent). Note that the elevated temperature signature curves (400, 600, 800 ºC) can be obtained, from their room-temperature counterpart (20 °C), through a "vertical translation" whose magnitude depends only on Young's modulus erosion caused by the temperature rise − therefore, the column buckling load natures and mode shapes corresponding to a given length are independent of the temperature value. Figure 3(b) exhibited the deformed shapes corresponding to the FT and D buckling modes at $L = L_{DG}$ = 1550 mm.

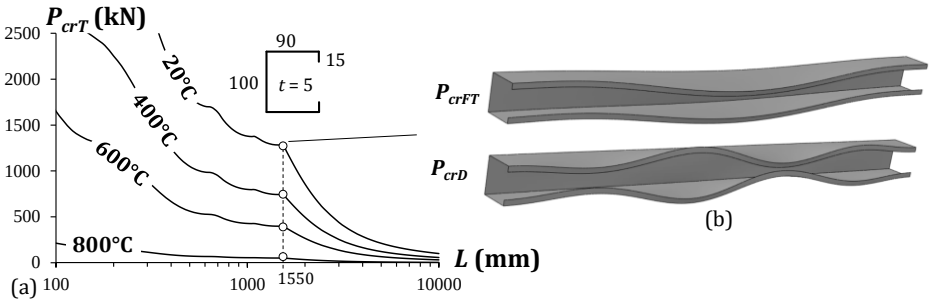

Figure 3. LC8 column buckling behavior: (a) P_{crT} *vs.* L signature curves for T = 20-400-600-800 ºC (AS/NZS-model, L in logarithmic scale) and (b) D and FT buckling modes related to $L = L_{DG}$.

3 Numerical model

The column D-FT post-buckling behavior and ultimate strength are determined utilizing ABAQUS [19] SFE GMNIA, with the same approach used in recent studies (e.g., [5], [6], [9]). Fine S4 element meshes with a length-to-width ratio close to 1 were adopted (S4 ABAQUS nomenclature – 4-node shell finite elements with six degrees of freedom per node and full integration), as suggested in [4]. The analysis strategy combines an incremental iterative Newton-Raphson's method with an arclength control strategy. They simulate the response of columns at uniform elevated temperature distributions (deemed engulfed in flames), thus sharing the surrounding air temperature [5] and subsequently axially compressed up to failure − steady-state analyses. The column fixed-ended support conditions are replicated by attaching the column-end cross-sections to rigid plates with all the degree of freedom restrained – except by the axial translations, thus enabling the imposition of small longitudinal displacements at the ended-section centroids (see Figure 4). Critical-mode FT initial geometrical imperfections

with amplitude $L/1000$ were imposed on all columns analyzed (the most detrimental shape [3], [4]). These mode shapes were preliminary obtained through ABAQUS elastic buckling analyses, conducted with the same SFE mesh subsequently employed to carry out the GMNIA − thus the buckling analysis output can be used as a GMNIA input[1]. Note that strain-hardening, residual stress and rounded corner strength effects were disregarded in this work since several authors (e.g., Ellobody and Young [20]) have shown that their combined influence on the column failure load is negligible.

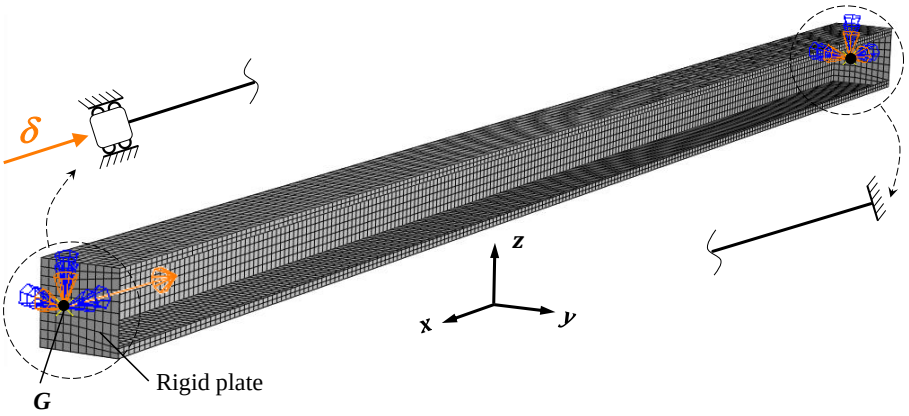

Figure 4. Column SFE models developed in this work.

3.1 Material model

ABAQUS [19] multi-linear stress-strain curve is used to insert AS/NZS [17] constitutive law into the models. As mentioned before, Figure 2(a) permits visualizing the temperature-dependence of Young's modulus and yield stress reduction factors ($k_E = E_T/E_{20}$ and $k_y = f_{yT}/f_y$, respectively) for low-strength steels (LSS, f_y < 450 MPa) and high strength steel (HSS, $f_y \geq 450$ MPa) – the k_y and k_E expressions are given in Table 2. Figure 2(b), shows the qualitative differences between LSS and HSS normalized stress-strain curves for T = 20-40-600 °C.

The stress-strain relationship provided in AS/NZS [17] is based on the Ramberg-Osgood model [21], Eq. (1). In this equation, the parameters β and η_T are associated with the type of steel (i.e., LSS or HSS). Besides, the code determines the stress-strain curves must be bi-linear (perfectly elastic-plastic) for LSS at $T \leq 200$ °C. For $T > 200$ °C as well as for HSS at 20°C $\leq T \leq$ 800°C, all the curves are completely non-linear – following Eq. (1). Note that, the AS/NZS [17] model is appliable for temperatures ranging from 20 °C to 800 °C and steels with yield stresses comprised between 250 MPa and 550 MPa – aiming to cover a wider range of slenderness, in this work, two exceptions are considered, steels with f_y = 150 MPa and f_y = 750 MPa.

$$\varepsilon_T = \frac{f_T}{E_T} + \beta\left(\frac{f_{yT}}{E_T}\right)\left(\frac{f_T}{f_{yT}}\right)^{\eta_T} \tag{1}$$

With:

Table 2. AS/NZS [17] constitutive model parameters for LSS and HSS.

Low-strength steel (LSS)	High-strength steel (HSS)
$\beta = 1.5$	$\beta = 0.86$
$\eta_T = 0.000138T^2 - 0.085468T + 19.212$	$\eta_T = -3.05 \cdot 10^{-7}T^3 - 0.0005T^2 - 0.2615T + 62.653$
$k_y = \begin{cases} -0.0005T + 1.01 & \text{if } 20°C \leq T < 200°C \\ 25(1.16 - T^{0.022}) & \text{if } 200°C \leq T \leq 800°C \end{cases}$	$k_y = \begin{cases} -0.000179T + 1.00358 & \text{if } 20°C \leq T < 300°C \\ -0.0028T + 1.79 & \text{if } 300°C \leq T < 600°C \\ -0.0004T + 0.35 & \text{if } 600°C \leq T \leq 800°C \end{cases}$
$k_E = \begin{cases} -0.000835T + 1.0167 & \text{if } 20\,°C \leq T \leq 200\,°C \\ -0.00135T + 1.1201 & \text{if } 200\,°C < T \leq 800\,°C \end{cases}$	

where, ε_T is the strain corresponding to an applied stress f_T, at temperature T, and f_{yT} and E_T are the yield stress and Young's modulus at temperature T, respectively.

[1] The numerical model was previously validated in [9] , but due to space limitations this topic will not be addressed here,

4 Elastic-plastic post-buckling behavior at elevated temperatures

This section addresses the influence of the elevated temperature on the elastic-plastic post-buckling behavior of selected CFS LC columns undergoing D-FT true interaction. Figure 5(a)-(b) shows the LC8 equilibrium paths P/P_{cr} *vs.* $(v+v_0)/t$ considering steels of 250 MPa and 550 MPa, subject to temperatures T = 20-100-200-300-400-500-600-700-800 ºC − $P_{cr} = \min\{P_{crG}; P_{crD}\}$ at T = 20°C (see Section 2), v is the mid-span bottom flange-lip corner vertical displacement and v_0 its initial value. The white circles emphasize the failure loads ($P_{uT} = A \cdot f_{uT}$). The columns' deformed shapes and plastic strain contours at collapse ($P = P_{uT}$) and at T = 20-400-600 ºC are also displayed. Since all columns presented qualitatively identical behaviors, only LC8 (R_{GD} = 1.0) results are presented and discussed here. The observation of these post-buckling results prompts the following remarks:

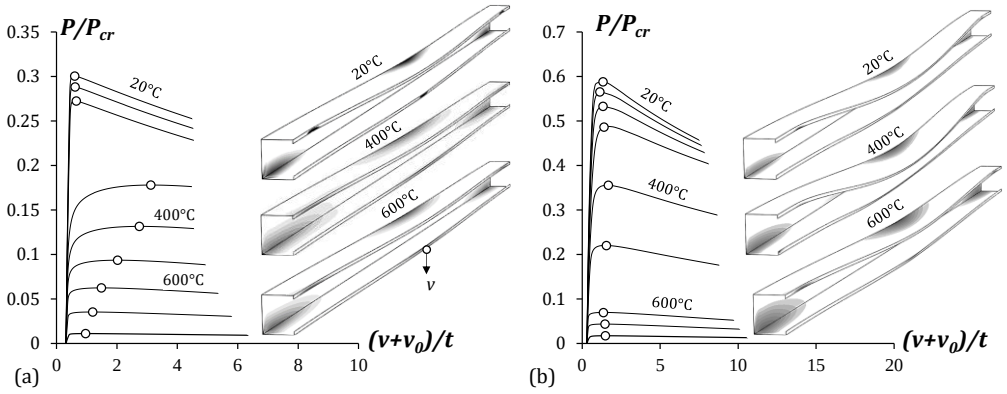

Figure 5. LC8 Elastic-plastic equilibrium paths P/P_{cr} *vs.* $(v+v_0)/t$ for all temperatures analyzed and failure modes at T = 20-400-600 °C: (a) f_y = 250 MPa (LSS) and (b) f_y = 550 MPa (HSS).

i) In general, the failure loads and equilibrium paths for both LSS and HSS columns decrease (move downwards) as the temperature rises – this effect stems from the yield stress and elastic modulus erosion (felt through k_y and k_E reduction factors).

ii) Figure 5 shows clear differences between the LSS and HSS column behaviors. For LSS, there are two distinct equilibrium paths: (ii_1) at T < 300°C columns reach the peak and fail abruptly, with small displacements, (ii_2) while for $T \geq$ 300 °C, the equilibrium paths are smoother, and the failures occur with larger displacements. (ii_3) For HSS, on the other hand, the curves are quite similar, with no noticeable substantial difference.

iii) Concerning the deformed shapes, both LSS and HSS columns present failure modes combining yielding at bottom web-flange and top flange-lip corners at the end cross-sections and top web-flange corners at the middle cross-section – note that HSS columns show larger displacements at failure. In addition, it is observable that the yielding zones for all columns "spread out" as the temperature rises, which can be attributed to strain hardening effects and the increasing non-linearity for elevated temperatures.

5 Failure load

The outputs of the parametric study conducted in this work consist of 864 analyses involving (i) 12 LC geometries, (ii) 9 uniform temperatures (20-100-200-300-400-500-600-700-800 °C) and (iii) 8 room-temperature (20 °C) yield stresses. The normalized failure loads are presented in Figure 6 (P_{uT}/P_{yT} *vs.* $\lambda_{FT.T}$ plots), which also exhibit the elastic buckling curve ($1/\lambda^2_{FT.T}$), for comparative purposes – the white and grey circles concern LSS and HSS columns` failure loads, respectively. Based on these results, it can be concluded that:

i) Regardless of the temperature, the P_{uT}/P_{yT} *vs.* $\lambda_{FT.T}$ "clouds" follow a "Winter-type" trend of strength curves, even if there is some "vertical dispersion" along the whole slenderness range considered.

ii) The failure loads are well merged for temperatures of 20-100-200-600-800 °C, with a small dispersion for T = 600 °C. For 300 °C ≤ T ≤ 500 °C, LSS failure loads are significantly lower than HSS ones in the low-to-moderate slenderness ranges ($\lambda_{FT.T}$ < 1.5).

iii) Note that the point "clouds" are condensed into a reduced slenderness range ($\lambda_{FT.T} \leq$ 1.5) for T = 600-700

°C. This happens due to the simultaneous variation of k_y and k_E, which leads to very close slenderness values for all steels considered in this study in these temperatures.

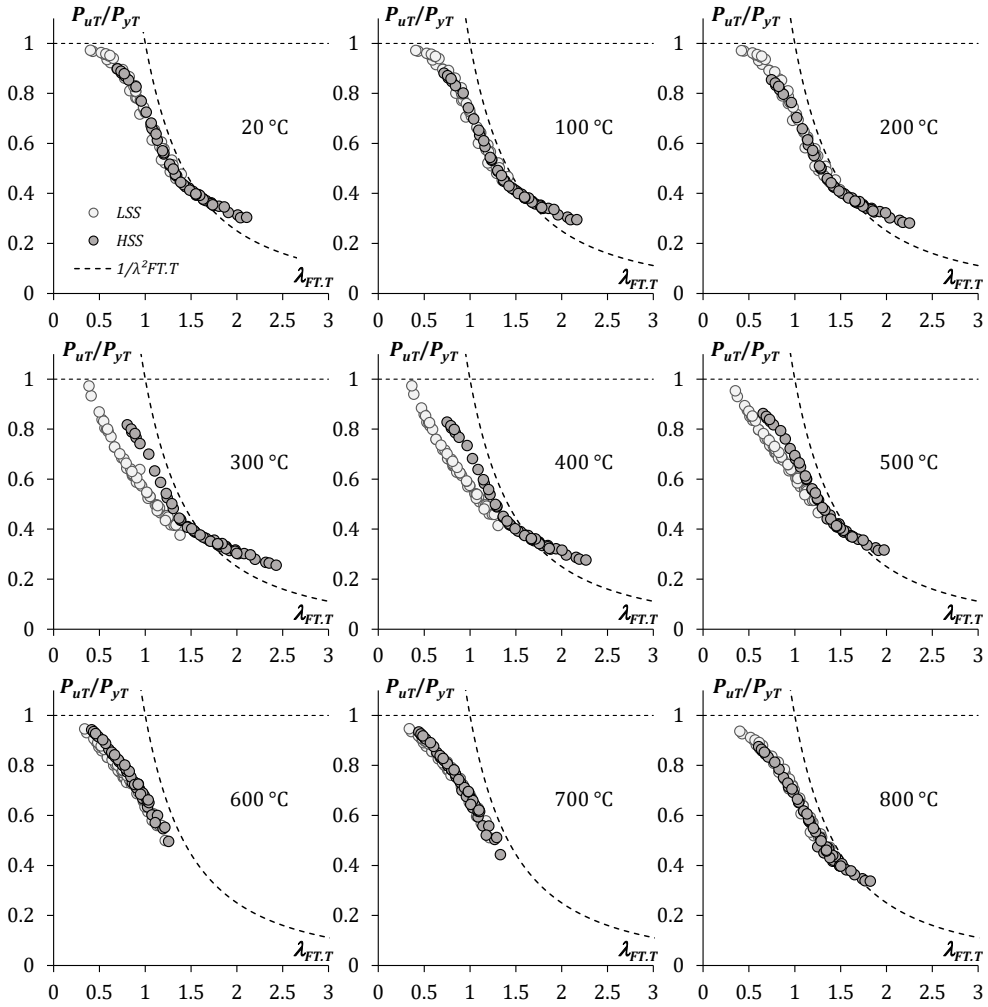

Figure 6. P_{uT}/P_{yT} *vs.* $\lambda_{FT.T}$ plots for all columns analyzed in this work (T = 20-800°C).

iv) Finally, it can be concluded that there is no significant drop in the point "clouds" curves as temperatures increase – the elastic buckling curves provide a good reference to this statement. In fact, the vertical dispersion between LSS and HSS column results seems to be more related to the increase in non-linearity of LSS stress-strain curves with temperature when compared to HSS ones. Similar findings were reported in [14], [16].

6 Conclusions

This work reported new results of an ongoing numerical investigation on the post-buckling behavior of cold-formed steel lipped-channel fixed-ended columns experiencing true distortional-global (flexural-torsional) interactions at room and elevated temperatures. A total of 864 failure load results concerning columns affected by TI at room and elevated temperatures were obtained. It was found that the failure loads of columns with low-strength steel or high-strength steel present a great variability (dispersion) for temperatures comprised between 300 °C and 600 °C, which indicates that the non-linearity of the AS/NZS 4600 stress-strain curves may play an important role in the column strength and behavior. These data will further be used to assess and provide modifications (if necessary) in the available DSM-based strength curves. Conclusively, it is worth noting that the findings reported in this work inspire the sake of a DSM-based design approach generalized for CFS lipped-channel columns affected by D-FT interaction at room and elevated temperatures.

Acknowledgements. The first two authors gratefully acknowledge the financial support of the Brazilian institutions (i) CAPES (Coordenação de Aperfeiçoamento de Pessoal de Nível Superior) – Finance Code 001 (both authors), (ii) CNPq (Conselho Nacional de Desenvolvimento Científico e Tecnológico) – Finance Codes 141021/2020-9 (first author) and 313197/2020-2 (second author) and (iii) FAPERJ (Fundação Carlos Chagas Filho de Amparo à Pesquisa do Estado do Rio de Janeiro) – Finance Code E-26/200.959/2021 (second author). The third author gratefully acknowledges the financial support of FCT (Fundação para a Ciência e a Tecnologia – Portugal) – project UIDB/04625/2020 (funding the research unit CERIS).

Authorship statement. The authors hereby confirm that they are the sole liable persons responsible for the authorship of this work, and that all material that has been herein included as part of the present paper is either the property (and authorship) of the authors, or has the permission of the owners to be included here.

References

[1] D. Camotim and P. B. Dinis, "Coupled instabilities with distortional buckling in cold-formed steel lipped channel columns," *Thin Walled Struct.*, vol. 49, no. 5, pp. 562–575, 2011, doi: 10.1016/j.tws.2010.09.003.

[2] P. B. Dinis and D. Camotim, "Post-buckling behaviour and strength of cold-formed steel lipped channel columns experiencing distortional / global interaction," vol. 89, pp. 422–434, 2011, doi: 10.1016/j.compstruc.2010.11.015.

[3] D. Camotim and P. B. Dinis, "Distortional-global interaction in lipped channel columns," *Proc. Inst. Civ. Eng. Struct. Build.*, vol. 166, no. 8, pp. 381–391, 2013, doi: 10.1680/stbu.12.00054.

[4] A. D. Martins, D. Camotim, and P. B. Dinis, "On the distortional-global interaction in cold-formed steel columns : Relevance , post-buckling behaviour , strength and DSM design," vol. 145, pp. 449–470, 2018, doi: 10.1016/j.jcsr.2018.02.031.

[5] A. Landesmann, D. Camotim, and F. C. M. Silva, "DSM Design of Cold-Formed Steel Columns Failing in Distortional Modes at Elevated Temperatures," *Int. J. Steel Struct.*, vol. 19, no. 3, pp. 1023–1041, 2019, doi: 10.1007/s13296-018-0184-x.

[6] A. A. Bicelli, A. Landesmann, D. Camotim, and P. B. Dinis, "Flexural–torsional failure and DSM design of fixed-ended cold-formed steel columns at elevated temperatures," *Thin-Walled Struct.*, vol. 169, no. August, p. 108362, 2021, doi: 10.1016/j.tws.2021.108362.

[7] B. W. Schafer, "Thin-Walled Structures Advances in the Direct Strength Method of cold-formed steel design," *Thin Walled Struct.*, vol. 140, no. April, pp. 533–541, 2019, doi: 10.1016/j.tws.2019.03.001.

[8] E. B. Ferreira FIlho, A. Landesmann, and D. Camotim, "Distortional-Global Interactive Failure and DSM Design of CFS Lipped Channel Columns at Elevated," in *The International Colloquium on Stability and Ductility of Steel Structures (SDSS)*, 2022, pp. 448–457.

[9] E. B. Ferreira Filho, A. Landesmann, and D. Camotim, "DSM design of CFS lipped channel columns undergoing distortional-global interaction at elevated temperatures," *Proc. Annu. Stab. Conf. Struct. Stab. Res. Counc. SSRC 2023*, vol. 1, no. d, pp. 1–44, 2023.

[10] CEN, *EN 1993-1-2, Eurocode 3: Design of steel structures - Part 1-2: General rules - Structural fire design.*, vol. 1, no. 2005. Brussels (Belgium): Comité Européen de Normalisation, 2005.

[11] T. Ranawaka and M. Mahendran, "Distortional buckling tests of cold-formed steel compression members at elevated temperatures," *J. Constr. Steel Res.*, vol. 65, no. 2, pp. 249–259, 2009, doi: 10.1016/j.jcsr.2008.09.002.

[12] T. Ranawaka and M. Mahendran, "Numerical modelling of light gauge cold-formed steel compression members subjected to distortional buckling at elevated temperatures," *Thin-Walled Struct.*, vol. 48, no. 4–5, pp. 334–344, 2010, doi: 10.1016/j.tws.2009.11.004.

[13] Y. B. Heva and M. Mahendran, "Flexural-torsional buckling tests of cold-formed steel compression members at elevated temperatures," *Steel Compos. Struct.*, vol. 14, no. 3, pp. 205–227, 2013, doi: https://doi.org/10.12989/scs.2013.14.3.205.

[14] S. Gunalan, Y. B. Heva, and M. Mahendran, "Flexural-torsional buckling behaviour and design of cold-formed steel compression members at elevated temperatures," *Eng. Struct.*, vol. 79, pp. 149–168, 2014, doi: 10.1016/j.engstruct.2014.07.036.

[15] M. Rokilan and M. Mahendran, "DSM design of CFS columns subject to distortional buckling at elevated temperatures," *Fire Saf. J.*, vol. 125, p. 103395, 2021, doi: 10.1016/j.firesaf.2021.103395.

[16] M. Rokilan and M. Mahendran, "Effects of nonlinear elevated temperature stress-strain characteristics on the global buckling capacities of cold-formed steel columns," *Thin-Walled Struct.*, vol. 160, no. December 2020, p. 107352, 2021, doi: 10.1016/j.tws.2020.107352.

[17] AS/NZS (Australian/New Zeland Standard), *Cold-formed Steel Structures*. Sidney-Wellington, 2018.

[18] R. Bebiano, D. Camotim, and R. Gonçalves, "GBTUL 2.0 − A second-generation code for the GBT-based buckling and vibration analysis of thin-walled members," *Thin-Walled Struct.*, vol. 124, no. August 2017, pp. 235–257, 2018, doi: 10.1016/j.tws.2017.12.002.

[19] "ABAQUS. Abaqus/Standard User's Manual, 2014, version 6.14-1." .

[20] E. Ellobody and B. Young, "Behavior of Cold-Formed Steel Plain Angle Columns," *J. Struct. Eng.*, vol. 131, no. 3, pp. 457–466, 2005, doi: 10.1061/(asce)0733-9445(2005)131:3(457).

[21] W. Ramberg and W. R. Osgood, "Description of Stress-strain curves by three parameters," 1943.